


Cite this: *RSC Adv.*, 2019, 9, 3429

Mn⁴⁺-activated Li₃Mg₂SbO₆ as an ultrabright fluoride-free red-emitting phosphor for warm white light-emitting diodes

Shaoying Wang, Qi Sun, Balaji Devakumar, Jia Liang, Liangling Sun and Xiaoyong Huang 

In this paper, we report on highly efficient Mn⁴⁺-activated double perovskite Li₃Mg₂SbO₆ (LMS) red-emitting phosphors. These LMS:Mn⁴⁺ phosphors can be efficiently excited over a broad wavelength band from 235 nm to 600 nm peaking at 344 nm and 469 nm, and exhibited an intense red emission band with a range from 600 nm to 800 nm centered around 651 nm. The optimal Mn⁴⁺ doping concentration of LMS:Mn⁴⁺ was 0.6 mol% and its internal quantum efficiency can reach as high as 83%. Besides, the thermal quenching effect on the optical property was also analyzed. Finally, a warm white light-emitting diode (WLED) lamp was fabricated by using a 454 nm InGaN blue LED chip combined with a blend of YAG:Ce³⁺ yellow phosphors and the as-prepared LMS:0.6% Mn⁴⁺ red phosphors, which showed bright white light with CIE chromaticity coordinates (0.4093, 0.3725), correlated color temperature (CCT = 3254 K), color rendering index (CRI = 81) and luminous efficacy (LE = 87 lm/W).

Received 11th December 2018

Accepted 19th January 2019

DOI: 10.1039/c8ra10158b

rsc.li/rsc-advances

1. Introduction

In the past decade, the research on white light-emitting diodes (WLEDs), which show numerous merits including low energy consumption, long working time, low cost, small volume, and environmental compatibility, is becoming a hotspot in the lighting and display fields.^{1–9} WLEDs are considered to replace the traditional fluorescent and incandescent lamps as the next-generation solid-state lighting source. Currently, the popular method to fabricate the commercial WLEDs is using the InGaN blue LED chips combined with YAG:Ce³⁺ yellow phosphors.^{10–13} Unfortunately, owing to the absence of red phosphors, such WLEDs exhibit cold white light accompanied with low color rendering index (CRI) as well as high correlated color temperature (CCT), which is unfavorable for their further application in indoor lighting.^{14–16} Hence, it is of great theoretical value and practical significance to seek red-emitting phosphors with good luminescent performance for fabricating warm WLEDs.

Up till now, the most studied red-emitting phosphors were activated by rare earth ions Eu³⁺ and Eu²⁺ owing to their preferable properties.¹⁷ However, there are some limitations in those red phosphors, for example, Eu³⁺ activated phosphors exhibit sharp excitation peaks in the near-ultraviolet (UV) and blue light region owing to its parity-forbidden 4f–4f transitions,^{18,19} while the preparation process of Eu²⁺ doped (oxy) nitrides is quite harsh, and the rare earth ions are normally expensive.^{20,21} In order to obtain the low-cost and easily

available red-emitting phosphors with good luminescent properties, the transition metal ions Mn⁴⁺ with 3d³ electronic configuration are regarded as alternative activators because the Mn⁴⁺-activated phosphors can be prepared on a mild condition and show broad absorption band in the near-UV or blue light region accompanied with deep red emission due to the spin-forbidden ²E_g → ⁴A_{2g} transition, the energy of which is highly dependent on the hybridization of Mn⁴⁺-ligand.^{22–24} Mn⁴⁺ ions are normally stable by occupying the cation sites in octahedral environments of the host materials such as fluorides and oxides.^{25,26} Recently, many Mn⁴⁺-activated fluorides (*i.e.*, A₂MF₆:Mn⁴⁺, A = Na, K, Rb, and Cs; M = Si, Ti, Ge, and Zr) have been investigated and they present a potential application for warm WLEDs, due to the suitable red emission peak locating at 620–640 nm because of the weak hybridization effect.^{27,28} Unfortunately, during the preparation process, the excessive use of hydrofluoric acid, which is harmful to the environment and health, limits their economic applications and industrial productions.²⁹ As an alternative, the environmentally friendly and chemically stable Mn⁴⁺ doped oxides (such as: Ba₂GdSbO₆:Mn⁴⁺,¹⁷ Ca₂YSbO₆:Mn⁴⁺,³⁰ and Mg₂TiO₄:Mn⁴⁺ (ref. 31)) have been discovered to be outstanding red converters for application in warm WLEDs, even if the red emission of Mn⁴⁺-doped oxides shifts to the deep-red region (>650 nm) due to the strong hybridization effect.³² As a double perovskite-type oxide, the compound Li₃Mg₂SbO₆ (LMS) possesses [SbO₆] octahedron and Mn⁴⁺ ions are expected to substitute the cationic sites of Sb⁵⁺ ions. However, so far the synthesis and luminescence properties of LMS:Mn⁴⁺ phosphors have not been reported.

College of Physics and Optoelectronics, Taiyuan University of Technology, Taiyuan 030024, P. R. China. E-mail: huangxy04@126.com

In this work, a series of novel high-efficiency Mn^{4+} -activated LMS phosphors were successfully synthesized. Under excitations by the near-UV light and blue light, the LMS:Mn^{4+} can exhibit intense red emission with high internal quantum efficiency (IQE). Furthermore, the crystal structure and optical properties of LMS:Mn^{4+} samples were investigated in detail. Finally, a prototype warm WLED lamp which generated bright white light was also successfully fabricated.

2. Experimental

$\text{Li}_3\text{Mg}_2\text{Sb}_{(1-x)}\text{O}_6:\text{xMn}^{4+}$ (abbreviated as: LMS:xMn^{4+}) phosphors were synthesized by a high-temperature solid-state reaction procedure. As the raw materials, Li_2CO_3 (analytical reagent, AR), MgO (AR), Sb_2O_5 (99.9%), and MnCO_3 (AR) were weighed in stoichiometric proportions and ground in an agate mortar. Then, the obtained powders were transferred into the alumina crucibles. Finally, the phosphors can be finally obtained after pre-firing at 600°C for 5 h and sintering again at 1200°C for 4 h in the air.

The phase purity was studied by X-ray diffraction patterns recorded on a diffractometer (Bruker D8) with $\text{Cu K}\alpha$ radiation ($\lambda = 1.54 \text{ \AA}$) in the 2θ range of $10\text{--}80^\circ$ at a step rate of 0.02° . Crystal structure was analyzed according to the Rietveld refinement performed using the FullProf program. The photoluminescence (PL) and PL excitation (PLE) spectra were measured with the excitation and emission slit width of 0.9 nm

as well as the dwell time of 0.1 s by a spectrometer (Edinburgh FS5) which was designed with plane gratings and equipped with a 150 W Xenon lamp. The decay curves were recorded on the spectrometer (Edinburgh FS5) with a pulsed Xenon lamp. The IQE and EQE were determined by the same spectrometer with an integrating sphere coated with BaSO_4 . The temperature-dependent PL spectra were also obtained on the spectrometer (Edinburgh FS5) equipped with a temperature controller. WLED devices were fabricated by coating the obtained phosphor-silicone on the surface of the LED chip. The as-fabricated WLEDs were operated by 3 V forward voltage with a driven current of 20 mA , and their electroluminescence (EL) spectra, luminous efficacy (LE), color rendering index (CRI), and correlated color temperature (CCT) were recorded by using an integrating-sphere spectroradiometer system (HAAS2000, Everfine).

3. Results and discussion

The XRD patterns of the LMS:xMn^{4+} phosphors ($x = 0.2\%$, 0.6% , and 1.2%) agreed well with the standard PDF card (JCPDS #36-1019) of the LMS host, shown in Fig. 1(a), indicating that Mn^{4+} ions were well incorporated into the LMS without any significant effects on the host crystal structure. In order to characterize the crystal structure of LMS:Mn^{4+} phosphors, the XRD Rietveld refinement for LMS:0.6\% Mn^{4+} sample was carried out and shown in Fig. 1(b).^{33,34} The refinement results

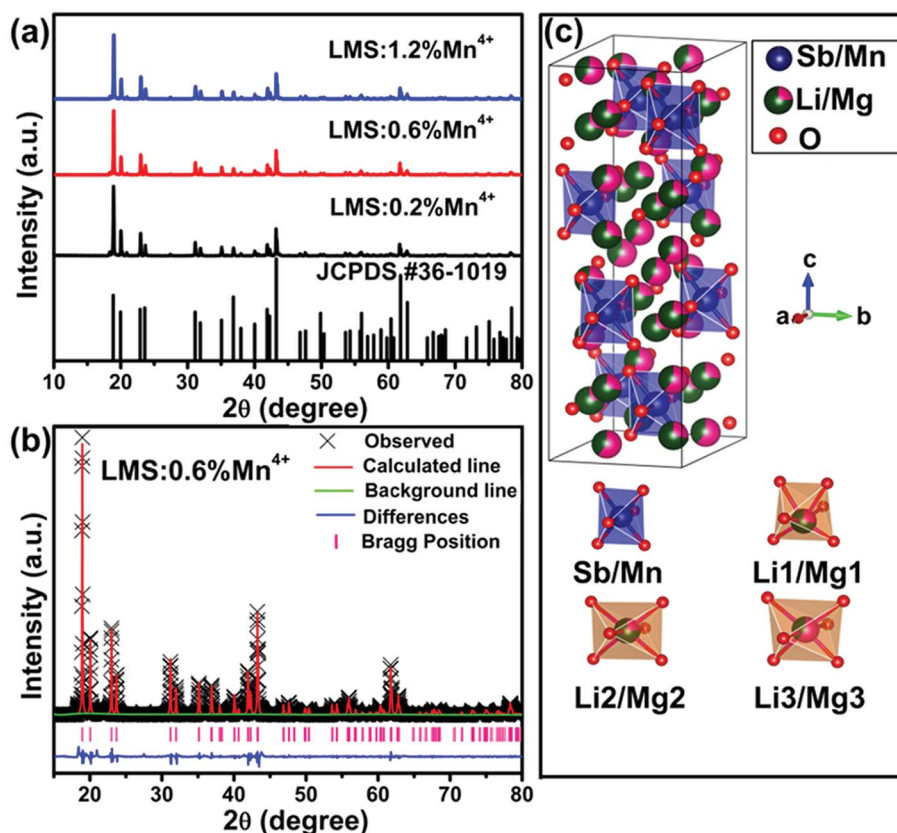


Fig. 1 (a) The XRD patterns of LMS:xMn^{4+} ($x = 0.2\%$, 0.6% , 1.2%) phosphors and the standard PDF card of the host LMS (JCPDS #36-1019). (b) The XRD Rietveld refinement for LMS:0.6\% Mn^{4+} . (c) The crystal structure of LMS:0.6\% Mn^{4+} .



including the cell parameters of LMS:0.6% Mn⁴⁺ determined to be $a = 8.6393(5) \text{ \AA}$, $b = 5.9262(4) \text{ \AA}$, $c = 17.8170(1) \text{ \AA}$, $\alpha = \beta = \gamma = 90^\circ$, and $V = 912.20(17) \text{ \AA}^3$ were achieved with the residual factors of $R_p = 9.36\%$, and $R_{wp} = 13.72\%$. Accordingly, the crystal structure of the LMS:0.6% Mn⁴⁺ was a partially ordered rock salt structure belonging to orthorhombic crystal system with a space group $Fddd$ (see Fig. 1(c)).³⁵ The crystal structure of LMS included four types of octahedrons, where Sb⁵⁺ ions completely occupied a group of octahedral sites and Li/Mg distributed non-randomly over other three groups of octahedral sites.³⁶ Here, it was more reasonable for Mn⁴⁺ ($r = 0.53 \text{ \AA}$) to substitute the Sb⁵⁺ ($r = 0.6 \text{ \AA}$) than Li⁺ ($r = 0.76 \text{ \AA}$) and Mg²⁺ ($r = 0.72 \text{ \AA}$) ions because of the closer radius.³⁷

Fig. 2(a) shows the PLE spectrum of LMS:0.6% Mn⁴⁺ phosphors. In the range of 235–600 nm, the PLE spectrum consisted of two broad excitation bands peaking at 344 nm attributed to the Mn–O charge transfer band (CTB) and the $^4A_{2g} \rightarrow ^4T_{1g}$ transition, as well as 469 nm owing to $^4A_{2g} \rightarrow ^4T_{2g}$ transition of Mn⁴⁺ ions with a monitoring wavelength of 651 nm, respectively,^{38–40} indicating that the phosphors can be excited by near-UV and blue light. Besides, there were some sharp PLE lines in the range of 450–500 nm due to the Xe lamp excitation source. The PL spectra of LMS:0.6% Mn⁴⁺ phosphors under 344 nm and 469 nm excitations were shown in Fig. 2(b). Evidently, the emission spectrum excited at 344 nm had the similar profile but the stronger emission intensity compared with that excited at 469 nm, and the PL spectra were composed of broad red emission bands in the range of 600–800 nm centered at around 651 nm, owing to the $^2E_g \rightarrow ^4A_{2g}$ transition of Mn⁴⁺ ions.^{41,42} Furthermore, the CIE chromaticity coordinates of LMS:0.6% Mn⁴⁺ under the excitation 344 nm and 469 nm were both calculated to be (0.724, 0.276), which located in red region. Moreover, the phosphors also exhibited bright red light under 365 nm UV lamp, as shown in the inset in Fig. 2(b).

Fig. 3(a) exhibits the emission spectra of LMS: x Mn⁴⁺ phosphors ($x = 0.1\%$, 0.2% , 0.4% , 0.6% , 0.8% , 1.0% and 1.2%) under 344 nm excitation. All the PL spectra exhibited similar emission profiles except that the PL intensities were different. Intuitively, the emission intensity of LMS: x Mn⁴⁺ as a function of Mn⁴⁺ concentration was shown in Fig. 3(b). When x increased from 0.1% to 1.2%, the emission intensity first increased to the

maximum with the optimal Mn⁴⁺ doping concentration $x = 0.6\%$ and then gradually decreased due to the concentration quenching effect.^{23,43} The concentration quenching effect was caused by the nonradiative energy transfer among Mn⁴⁺ ions.⁴⁴ And the critical distance (R_c) can be evaluated by the following equation to determine the energy transfer mechanism among Mn⁴⁺ ions for the concentration quenching:^{45,46}

$$R_c = 2 \left(\frac{3V}{4\pi x_c Z} \right)^{1/3} \quad (1)$$

where x_c , V , and Z represent the critical content, the volume of unit cell, and the number of cations that can be substituted by Mn⁴⁺ ions per unit cell, respectively. For LMS:0.6% Mn⁴⁺, $x_c = 0.6\%$, $Z = 8$, and $V = 912.20 (17) \text{ \AA}^3$, and thus the R_c was calculated to be around 33.11 \AA . The exchange interaction will take place when R_c value is shorter than 5 \AA . Therefore, the electric multipolar interaction played an important role in concentration quenching effect for LMS:Mn⁴⁺ phosphors. It is worth noting that the actual R_c value should be smaller than the calculated one because clustering will occur when Mn⁴⁺ show concentration quenching at a low concentration.

The specific type of the energy transfer mechanism can be further deduced using the following formula:^{47,48}

$$\log(I/x) = A - (\theta/3)\log x \quad (2)$$

where I refers to the emission intensity, x represents the concentration of dopants, A is a constant, and the electric multipole index $\theta = 3, 6, 8$, and 10 corresponds to the mechanism: nonradiative energy transfer among the nearest-neighbor ions, electric dipole–dipole, dipole–quadrupole, and quadrupole–quadrupole interaction, respectively.^{49–51} The relation between $\log(I/x)$ and $\log(x)$ was shown in Fig. 3(c), in which the experimental data can be well fitted to a straight line with R^2 value of 0.998 and a slope $(-\theta/3)$ of -1.27 . Hence, θ was calculated to be 3.81, which approached to 3, indicating that the primary type of the energy transfer mechanism among the Mn⁴⁺ activators in LMS:Mn⁴⁺ phosphors was the nonradiative energy transfer among the nearest-neighbor ions.

Fig. 3(d) illustrates the decay curves of the 651 nm emissions of LMS: x Mn⁴⁺ phosphors excited at 344 nm. The decay curves can be well fitted by a single-exponential function as below:⁵²

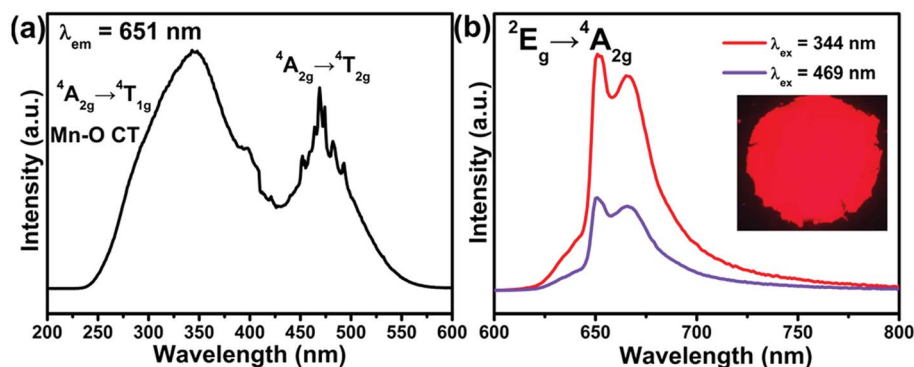


Fig. 2 (a) The PLE spectrum of LMS:0.6% Mn⁴⁺ phosphors monitored at 651 nm. (b) The PL spectra of LMS:0.6% Mn⁴⁺ phosphors ($\lambda_{ex} = 344$ and 469 nm) and the digital photograph under 365 nm near-UV lamp.



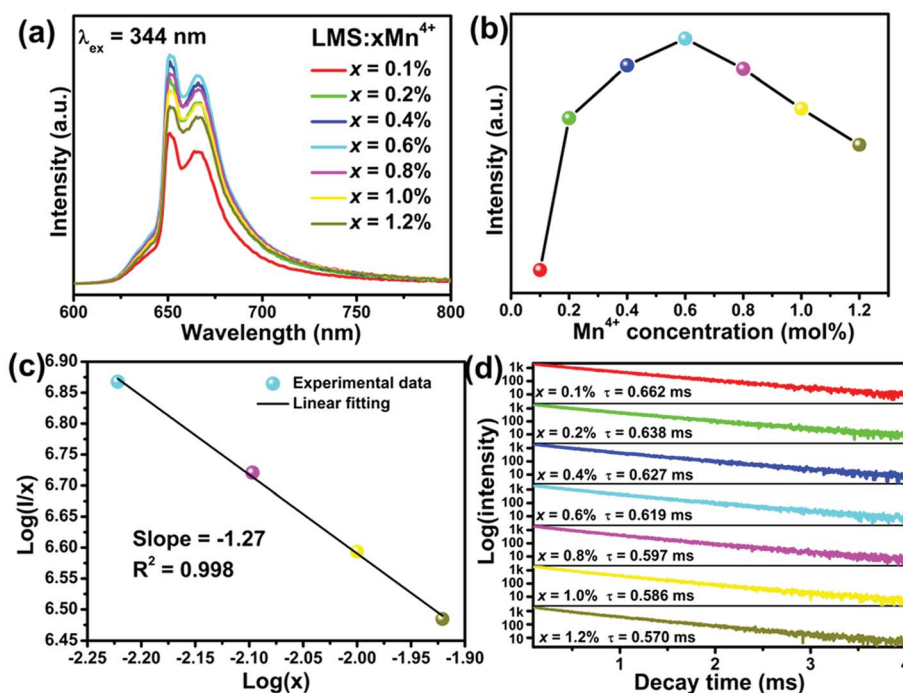


Fig. 3 (a) The PL spectra of LMS:xMn⁴⁺ phosphors under 344 nm excitation. (b) The diagram for emission intensity of LMS:xMn⁴⁺ depending on Mn⁴⁺ doping concentration. (c) The plot of log(I/x) versus log(x). (d) The decay curves of LMS:xMn⁴⁺ phosphors excited at 344 nm when monitored at 651 nm.

$$I_t = I_0 + A \exp(-t/\tau) \quad (3)$$

where I_0 and I_t refer to the initial emission intensity as well as the emission intensity at time t , respectively, A represents a constant, and τ refers to the lifetime. The lifetimes of the LMS:xMn⁴⁺ phosphors with the Mn⁴⁺ concentrations of 0.1%, 0.2%, 0.4%, 0.6%, 0.8%, 1.0%, and 1.2% were determined to be around 0.662, 0.638, 0.627, 0.619, 0.597, 0.586, and 0.570 ms, respectively. Clearly, when the concentration of Mn⁴⁺ ions increased, the lifetimes showed a downward tendency, because that the enhanced Mn⁴⁺ concentration made the distance between activators become much closer, thus raising the probability of energy transfer between Mn⁴⁺ ions.⁵³

Importantly, the IQE and EQE of the LMS:0.6Mn⁴⁺ phosphors can be determined by the following expressions:^{54,55}

$$\text{IQE} = \int L_S / (\int E_R - \int E_S) \quad (4)$$

$$\varepsilon = (\int E_R - \int E_S) / \int E_R \quad (5)$$

$$\text{EQE} = \varepsilon \times \text{IQE} \quad (6)$$

where $\int L_S$ is the integrated value of emission spectrum of LMS:0.6% Mn⁴⁺; $\int E_S$ and $\int E_R$ are the integrated values of the spectra for excitation light with and without sample in the integrating sphere, respectively; ε represents the absorption efficiency. Therefore, both the IQEs of LMS:0.6% Mn⁴⁺ phosphors excited at 344 nm and 469 nm were found to be about 83%. Furthermore, under 344 and 469 nm excitations, the corresponding EQEs were calculated to be 58% and 26%, respectively.

Fig. 4(a) shows the temperature-dependent emission spectra of LMS:0.6% Mn⁴⁺ phosphor with the temperature range of 303–443 K under the 344 nm excitation. There were no shifts in the emission peaks, while the emission intensity decreased a little rapidly with increasing the temperature, owing to the severe thermal quenching effect. The activation energy (ΔE) can be calculated based on the Arrhenius equation:⁵⁶

$$\ln(I_0/I - 1) = \ln C - \Delta E/kT \quad (7)$$

where I_0 and I correspond to the integrated values of emission spectra at initial temperature and operated temperature (T), respectively. C refers to a constant and k is the Boltzmann constant. The plot of $\ln(I_0/I - 1)$ versus $1/kT$ was exhibited in Fig. 4(b), which was well fitted to a line with $R^2 = 0.9983$ and a slope of -0.3725 . Therefore, the ΔE for thermal quenching was determined to be 0.3725 eV.

Consequently, the potential application of LMS:Mn⁴⁺ red phosphors were evaluated by comparing two types of WLED devices. Fig. 5(a) and (b) exhibit the electroluminescence (EL) spectra of the two as-fabricated WLED lamps. Owing to the absence of red phosphors, the LED device fabricated by using a 454 nm InGaN blue chip combined with only YAG:Ce³⁺ yellow phosphors possessed a lower R_a (i.e., the value of CRI) of 74.8 than that fabricated by using InGaN blue chip combined with a blend of YAG:Ce³⁺ yellow phosphors and LMS:0.6% Mn⁴⁺ red phosphors ($R_a = 81$). More importantly, the addition of LMS:0.6% Mn⁴⁺ red phosphors into the WLED device resulted in warm white light with CIE chromaticity coordinates (0.4093, 0.3725) and CCT = 3254 K, as shown in Fig. 5(c). Normally, the LE decreased when mixing the



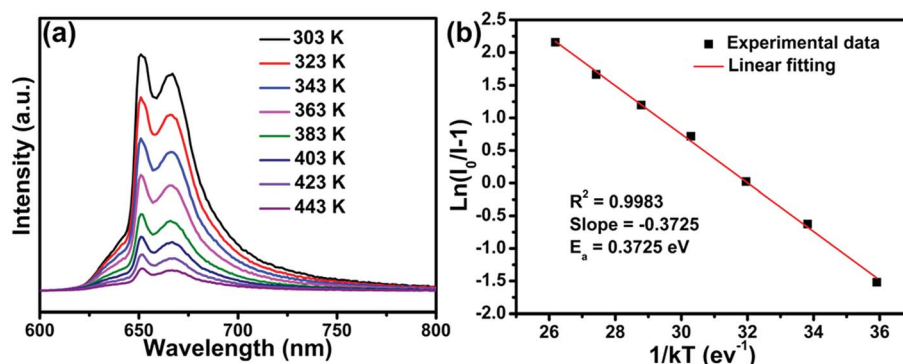


Fig. 4 (a) The temperature-dependent PL spectra of LMS:0.6% Mn^{4+} phosphor ranging from 303 to 443 K. (b) The dependence of $\ln(I_0/I - 1)$ on $1/kT$.

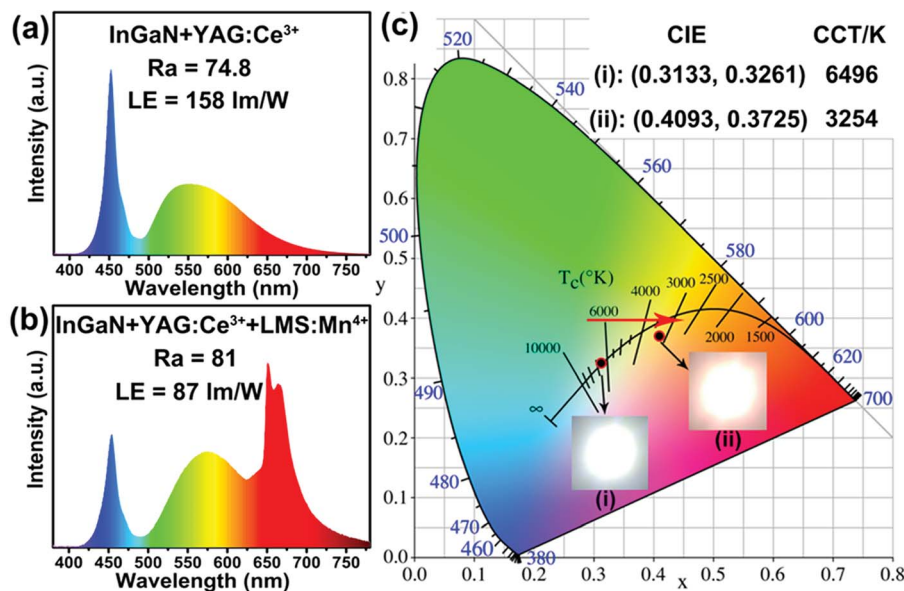


Fig. 5 EL spectra of the fabricated (a) cold WLED lamp (InGaN chip + YAG: Ce^{3+} yellow phosphors) and (b) warm WLED lamp (InGaN chip + YAG: Ce^{3+} yellow phosphors + LMS: Mn^{4+} red phosphors) driven by 20 mA current. (c) CIE chromaticity diagram of the fabricated WLED lamps. The insets are photographs of the WLED lamps.

red components into the LED devices due to the Stokes shifting and the weak sensitivity of human eyes to red light, which can explain that the LE of the cold white LED lamp ($\text{LE} = 158 \text{ lm W}^{-1}$) was much higher than that of the warm WLED lamp ($\text{LE} = 87 \text{ lm W}^{-1}$).⁵⁷ Even so, the LE value was higher than that of some warm WLEDs fabricated using the Mn^{4+} activated oxides or fluorides red phosphors which were reported before such as $\text{Sr}_2\text{MgGe}_2\text{O}_7:\text{Mn}^{4+}$ ($\text{LE} = 78.7 \text{ lm W}^{-1}$),⁵⁸ $\text{Ca}_{14}\text{Zn}_6\text{Ga}_{10}\text{O}_{35}:\text{Mn}^{4+}$ ($\text{LE} = 64.83 \text{ lm W}^{-1}$),⁵² $\text{Gd}_2\text{ZnTiO}_6:\text{Mn}^{4+}$ ($\text{LE} = 1.8 \text{ lm W}^{-1}$),²² $\text{Na}_3\text{AlF}_6:\text{Mn}^{4+}$ ($\text{LE} = 70 \text{ lm W}^{-1}$),⁵⁹ $\text{Na}_3\text{GaF}_6:\text{Mn}^{4+}$ ($\text{LE} = 56.73 \text{ lm W}^{-1}$),⁶⁰ and $\text{K}_2\text{LiGaF}_6:\text{Mn}^{4+}$ ($\text{LE} = 53.3 \text{ lm W}^{-1}$).⁶¹ These results confirmed that the LMS: Mn^{4+} red phosphors had a promising application in warm WLEDs.

4. Conclusions

To sum up, in this work, we reported novel highly efficient red-emitting LMS: Mn^{4+} phosphors. When excited at 344 nm and 469 nm, the LMS: Mn^{4+} phosphors can generate red emission

with the peak locating at around 651 nm in the range of 600–800 nm, corresponding to the ${}^2\text{E}_g \rightarrow {}^4\text{A}_{2g}$ transition of Mn^{4+} ions. This LMS: Mn^{4+} phosphor with the optimal concentration 0.6 mol% possessed high IQE up to 83%. And the impact of temperature on the luminescence property was also investigated. Moreover, the fabricated WLED lamp by using the InGaN blue chip coated with a blend of YAG: Ce^{3+} yellow phosphors and the as-prepared LMS:0.6% Mn^{4+} red phosphors showed warm white light with a higher CRI value (~ 81) and lower CCT value ($\sim 3254 \text{ K}$) than that fabricated without the red phosphors ($R_a = 74.8$, CCT = 6496 K). All the results exhibited above indicated that LMS: Mn^{4+} phosphors were promising red components for warm WLEDs.

Conflicts of interest

There are no conflicts to declare.



Acknowledgements

This work was supported by the National Natural Science Foundation of China (No. 51502190), the Program for the Outstanding Innovative Teams of Higher Learning Institutions of Shanxi.

References

- 1 X. Huang, *Nat. Photonics*, 2014, **8**, 748–749.
- 2 D. L. Dexter, *J. Chem. Phys.*, 1953, **21**, 836–850.
- 3 X. Huang, B. Li and H. Guo, *J. Alloys Compd.*, 2017, **695**, 2773–2780.
- 4 N. Narendran, Y. Gu, J. P. Freyssonier, H. Yu and L. Deng, *J. Cryst. Growth*, 2004, **268**, 449–456.
- 5 B. Wang, H. Lin, J. Xu, H. Chen and Y. Wang, *ACS Appl. Mater. Interfaces*, 2014, **6**, 22905–22913.
- 6 B. Li, X. Huang, H. Guo and Y. Zeng, *Dyes Pigm.*, 2018, **150**, 67–72.
- 7 H. Guo, X. Huang and Y. Zeng, *J. Alloys Compd.*, 2018, **741**, 300–306.
- 8 F. Baur and T. Jüstel, *J. Lumin.*, 2016, **177**, 354–360.
- 9 L. Meng, L. Liang and Y. Wen, *J. Mater. Sci.: Mater. Electron.*, 2014, **25**, 2676–2681.
- 10 P. Du, X. Huang and J. S. Yu, *Chem. Eng. J.*, 2018, **337**, 91–100.
- 11 S. Li, X. Wei, K. Deng, X. Tian, Y. Qin, Y. Chen and M. Yin, *Curr. Appl. Phys.*, 2013, **13**, 1288–1291.
- 12 W. Lü, Y. Jia, Q. Zhao, W. Lv and H. You, *Chem. Commun.*, 2014, **50**, 2635–2637.
- 13 P. Pust, P. J. Schmidt and W. Schnick, *Nat. Mater.*, 2015, **14**, 454–458.
- 14 Y. Liang, H. M. Noh, W. Ran, S. H. Park, B. C. Choi, J. H. Jeong and K. H. Kim, *J. Alloys Compd.*, 2017, **716**, 56–64.
- 15 X. Huang, S. Wang, B. Li, Q. Sun and H. Guo, *Opt. Lett.*, 2018, **43**, 1307–1310.
- 16 A. A. Setlur, E. V. Radkov, C. S. Henderson, J.-H. Her, A. M. Srivastava, N. Karkada, M. S. Kishore, N. P. Kumar, D. Aesram, A. Deshpande, B. Kolodin, L. S. Grigorov and U. Happek, *Chem. Mater.*, 2010, **22**, 4076–4082.
- 17 J. Zhong, S. Zhou, D. Chen, J. Li, Y. Zhu, X. Li, L. Chen and Z. Jia, *Dalton Trans.*, 2018, **47**, 8248–8256.
- 18 X. Zhang, L. Zhou and M. Gong, *Opt. Mater.*, 2013, **35**, 993–997.
- 19 Y. Shi, B. Liu, B. Liu, C. Li and Z. Wang, *RSC Adv.*, 2015, **5**, 95953–95959.
- 20 P. F. Smet, A. B. Parmentier and D. Poelman, *J. Electrochem. Soc.*, 2011, **158**, R37–R54.
- 21 T. Takeda, R.-J. Xie, T. Suehiro and N. Hirosaki, *Prog. Solid State Chem.*, 2018, **51**, 41–51.
- 22 H. Chen, H. Lin, Q. Huang, F. Huang, J. Xu, B. Wang, Z. Lin, J. Zhou and Y. Wang, *J. Mater. Chem. C*, 2016, **4**, 2374–2381.
- 23 M. G. Brik and A. M. Srivastava, *J. Lumin.*, 2013, **133**, 69–72.
- 24 S. Zhang, Y. Hu, H. Duan, L. Chen, Y. Fu, G. Ju, T. Wang and M. He, *RSC Adv.*, 2015, **5**, 90499–90507.
- 25 M. H. Du, *J. Mater. Chem. C*, 2014, **2**, 2475–2481.
- 26 Q. Peng, R. Cao, Y. Ye, S. Guo, Z. Hu, T. Chen and G. Zheng, *J. Alloys Compd.*, 2017, **725**, 139–144.
- 27 A. G. Paulusz, *J. Electrochem. Soc.*, 1973, **120**, 942–947.
- 28 H.-D. Nguyen and R.-S. Liu, *J. Mater. Chem. C*, 2016, **4**, 10759–10775.
- 29 Y. Arai and S. Adachi, *J. Lumin.*, 2011, **131**, 2652–2660.
- 30 J. Zhong, D. Chen, X. Chen, K. Wang, X. Li, Y. Zhua and Z. Jia, *Dalton Trans.*, 2018, **47**, 6528–6537.
- 31 C.-S. Huang, C.-L. Huang, Y.-c. Liu, S.-k. Lin, T.-S. Chan and H.-W. Tu, *Chem. Mater.*, 2018, **30**, 1769–1775.
- 32 T. S. Sreena, P. P. Rao, A. K. V. Raj and T. R. A. Thara, *J. Alloys Compd.*, 2018, **751**, 148–158.
- 33 K. Mommaa and F. Izumi, *J. Appl. Crystallogr.*, 2011, **44**, 1272–1276.
- 34 K. Mommaa and F. Izumi, *J. Appl. Crystallogr.*, 2008, **41**, 653–658.
- 35 G. C. Mather, R. I. Smith, J. M. S. Skakle, J. G. Fletcher, M. A. R. Castellanos, M. P. Gutierrez and A. R. West, *J. Mater. Chem.*, 1995, **5**, 1177–1182.
- 36 J. M. S. Skakle, M. A. Castellanos R., S. T. Tovar and A. R. West, *J. Solid State Chem.*, 1997, **131**, 115–120.
- 37 R. D. Shannon, *Acta Crystallogr.*, 1976, **32**, 751–767.
- 38 Q. Sun, B. Li, S. Wang, H. Guo and X. Huang, *J. Mater. Sci.: Mater. Electron.*, 2018, **29**, 12972–12977.
- 39 S. J. Kim, H. S. Jang, S. Unithrattil, Y. H. Kim and W. B. Im, *J. Lumin.*, 2016, **172**, 99–104.
- 40 L. Qin, S. Bi, P. Cai, C. Chen, J. Wang, S. I. Kim, Y. Huang and H. J. Seo, *J. Alloys Compd.*, 2018, **755**, 61–66.
- 41 X. Huang and H. Guo, *Dyes Pigm.*, 2018, **152**, 36–42.
- 42 J. Liang, L. Sun, B. Devakumar, S. Wang, Q. Sun, H. Guo, B. Li and X. Huang, *RSC Adv.*, 2018, **8**, 27144–27151.
- 43 A. Fu, L. Zhou, S. Wang and Y. Li, *Dyes Pigm.*, 2018, **148**, 9–15.
- 44 U. B. Humayoun, S. N. Tiruneh and D.-H. Yoon, *Dyes Pigm.*, 2018, **152**, 127–130.
- 45 X. Huang, H. Guo and B. Li, *J. Alloys Compd.*, 2017, **720**, 29–38.
- 46 X. Ding, G. Zhu, W. Geng, Q. Wang and Y. Wang, *Inorg. Chem.*, 2016, **55**, 154–162.
- 47 Y. Jin, Y. Hu, H. Wu, H. Duan, L. Chen, Y. Fu, G. Ju, Z. Mu and M. He, *Chem. Eng. J.*, 2016, **288**, 596–607.
- 48 L. G. V. Uitert, *J. Electrochem. Soc.*, 1967, **114**, 1048–1053.
- 49 R. Yu, H. M. Noh, B. K. Moon, B. C. Choi, J. H. Jeong, K. Jang, S. S. Yi and J. K. Jang, *J. Alloys Compd.*, 2013, **576**, 236–241.
- 50 D. Deng, H. Yu, Y. Li, Y. Hua, G. Jia, S. Zhao, H. Wang, L. Huang, Y. Li, C. Li and S. Xu, *J. Mater. Chem. C*, 2013, **1**, 3194–3199.
- 51 G. Blasse, *Phys. Lett. A*, 1968, **28**, 444–445.
- 52 C. Yang, Z. Zhang, G. Hu, R. Cao, X. Liang and W. Xiang, *J. Alloys Compd.*, 2017, **694**, 1201–1208.
- 53 K. Li, H. Lian and R. V. Deun, *Dalton Trans.*, 2017, **47**, 2501–2505.
- 54 H. Ji, L. Wang, Y. Cho, N. Hirosaki, M. S. Molokeev, Z. Xia, Z. Huang and R.-J. Xie, *J. Mater. Chem. C*, 2016, **4**, 9872–9878.
- 55 X. Ji, J. Zhang, Y. Li, S. Liao, X. Zhang, Z. Yang, Z. Wang, Z. Qiu, W. Zhou, L. Yu and S. Lian, *Chem. Mater.*, 2018, **30**, 5137–5147.
- 56 X. Huang, J. Liang, B. Li, L. Sun and J. Lin, *Opt. Lett.*, 2018, **43**, 3305–3308.



- 57 Y. Jin, M. H. Fang, M. Grinberg, S. Mahlik, T. Lesniewski, M. G. Brik, G. Y. Luo, J. G. Lin and R. S. Liu, *ACS Appl. Mater. Interfaces*, 2016, **8**, 11194–11203.
- 58 W. Chen, Y. Cheng, L. Shen, C. Shen, X. Liang and W. Xiang, *J. Alloys Compd.*, 2018, **762**, 688–696.
- 59 E. H. Song, J. Q. Wang, S. Ye, X. F. Jiang, M. Y. Peng and Q. Y. Zhang, *J. Mater. Chem. C*, 2016, **4**, 2480–2487.
- 60 T. T. Deng, E. H. Song, J. Sun, L. Y. Wang, Y. Deng, S. Ye, J. Wang and Q. Y. Zhang, *J. Mater. Chem. C*, 2017, **5**, 2910–2918.
- 61 Y. Zhu, J. Yu, Y. Liu, M. G. Brik, L. Huang, T. Xuan and J. Wang, *RSC Adv.*, 2017, **7**, 30588–30593.

